

Burial and Exhumation of Sedimentary Rocks Revealed by the Base Stimson Erosional Unconformity, Gale Crater, Mars

**Key Points:**

- Paleotopographic mapping is consistent with an erosional unconformity between the Mt. Sharp group and Stimson formation
- Lateral variations in paleorelief are regionally present along the contact at the base of the Stimson formation
- Erosion and exhumation were likely driven by eolian processes and a transition from wet to dry climate transition

Correspondence to:

J. A. Watkins,
Jessica.a.watkins@nasa.gov

Citation:

Watkins, J. A., Grotzinger, J. P., Stein, N. T., Banham, S. G., Gupta, S., Rubin, D. M., et al. (2022). Burial and exhumation of sedimentary rocks revealed by the base Stimson erosional unconformity, Gale crater, Mars. *Journal of Geophysical Research: Planets*, 127, e2022JE007293. <https://doi.org/10.1029/2022JE007293>

Received 12 MAR 2022

Accepted 22 APR 2022

Author Contributions:

Conceptualization: Jessica A. Watkins, John P. Grotzinger, Sanjeev Gupta, David M. Rubin, Kathryn Stack Morgan

Data curation: Nathan T. Stein, Jens Frydenvang

Formal analysis: Jessica A. Watkins, John P. Grotzinger, Nathan T. Stein, Steven G. Banham, Kathryn Stack Morgan, Jens Frydenvang, Kirsten L. Siebach, Michael P. Lamb, Dawn Y. Sumner, Kevin W. Lewis

Funding acquisition: John P. Grotzinger

Investigation: Jessica A. Watkins, John P. Grotzinger, Nathan T. Stein, Sanjeev Gupta, David M. Rubin, Kathryn Stack Morgan, Kenneth S. Edgett, Jens Frydenvang, Kirsten L. Siebach, Michael P. Lamb, Dawn Y. Sumner, Kevin W. Lewis

Jessica A. Watkins^{1,2} , John P. Grotzinger¹ , Nathan T. Stein¹, Steven G. Banham³ , Sanjeev Gupta³, David M. Rubin⁴ , Kathryn Stack Morgan⁵, Kenneth S. Edgett⁶ , Jens Frydenvang⁷, Kirsten L. Siebach⁸ , Michael P. Lamb¹, Dawn Y. Sumner⁹ , and Kevin W. Lewis¹⁰ 

¹Division of Geological and Planetary Sciences, California Institute of Technology, Pasadena, CA, USA, ²Now at NASA Johnson Space Center, Houston, TX, USA, ³Department of Earth Science and Engineering, Imperial College, London, UK, ⁴Department of Earth and Planetary Sciences, University of California, Santa Cruz, Santa Cruz, CA, USA, ⁵Jet Propulsion Laboratory, California Institute of Technology, Pasadena, CA, USA, ⁶Malin Space Science Systems, San Diego, CA, USA, ⁷Globe Institute, University of Copenhagen, Copenhagen, Denmark, ⁸Department of Earth, Environmental, and Planetary Sciences, Rice University, Houston, TX, USA, ⁹Geology Department, University of California, Davis, Davis, CA, USA, ¹⁰Department of Earth and Planetary Sciences, Johns Hopkins University, Baltimore, MD, USA

Abstract Sedimentary rocks record the ancient climate of Mars through changes between subaqueous and eolian depositional environments, recognized by their stratal geometries and suites of sedimentary structures. Orbiter- and rover-image-based geologic mapping show a dynamic evolution of the 5-km-thick sedimentary sequence exposed along the flanks of Aeolis Mons (informally, Mt. Sharp) in Gale crater, Mars, by deposition of subaqueous strata followed by exhumation via eolian erosion and then deposition of overlying, onlapping strata of inferred eolian origin. This interpretation suggests that a significant unconformity should occur at the base of the onlapping strata, thus predicting lateral variations in elevation along the contact between the underlying Mt. Sharp group and overlying Stimson formation. Curiosity rover and high-resolution orbital image data quantify paleotopographic variability associated with the contact; ~140 m of net elevation change and a slope closely aligned with the modern topography is expressed along the regional contact. These results support the interpretation of an erosional unconformity between these strata and that it was likely formed as a result of eolian erosion within the crater, indicative of a transition from wet to dry climate and providing insight into the stratigraphic context, geologic history, and habitability within Gale crater.

Plain Language Summary The discovery of sedimentary rocks on Mars is relatively recent. On a planet that apparently lacked plate tectonics, one important question is whether or not there is a rock cycle in which sediments become rocks that then are exhumed and recycled back into the crust through renewed burial. Rover missions have confirmed the existence of the first part of this cycle—erosion, transport, deposition, and burial. However, the second half of the cycle, which begins with exhumation, is poorly constrained. The work presented here demonstrates the presence of ancient surfaces of erosion—unconformities—that mark past exhumation events at Gale crater. Furthermore, the ancient erosion surface is then overlain by a younger series of sedimentary rocks, which demonstrates burial of that unconformity surface and the completion of the rock cycle. On Earth, exhumation is driven by tectonic uplift, followed by erosion via rainfall and fluvial processes; on Mars, exhumation was driven entirely by eolian erosion and deflation. Understanding the sedimentary rock cycle is especially significant in the search for ancient biosignatures on Mars as virtually all remnants of Earth's earliest biosphere are preserved in sedimentary rocks that were formed in this fashion.

1. Introduction

Understanding the cycle of sediments to become sedimentary rocks that might preserve organic compounds and biosignatures, and how these rocks then become exposed at the surface for study and sampling, is essential to guide rover exploration. The Curiosity rover benefitted from this knowledge in its discovery of preserved organics (Eigenbrode et al., 2018; Freissinet et al., 2015). The study of sedimentary rocks and processes on Mars, as on Earth, must necessarily involve analysis of the characteristic attributes of strata as well as their bounding surfaces, which in all cases represent some degree of temporal discontinuity (Sadler, 1981). Early studies of Martian strata showed that sedimentation was discontinuous, as revealed, for example, by the break in accumulation implied

© 2022. The Authors.

This is an open access article under the terms of the [Creative Commons Attribution-NonCommercial-NoDerivs License](https://creativecommons.org/licenses/by/4.0/), which permits use and distribution in any medium, provided the original work is properly cited, the use is non-commercial and no modifications or adaptations are made.

Methodology: Jessica A. Watkins, John P. Grotzinger, Nathan T. Stein, Jens Frydenvang, Kirsten L. Siebach, Michael P. Lamb, Dawn Y. Sumner, Kevin W. Lewis

Project Administration: John P. Grotzinger

Resources: John P. Grotzinger
Software: Nathan T. Stein

Supervision: John P. Grotzinger

Validation: Jessica A. Watkins, John P. Grotzinger, Nathan T. Stein, Sanjeev Gupta, Kathryn Stack Morgan, Kenneth S. Edgett, Kirsten L. Siebach, Michael P. Lamb, Dawn Y. Sumner, Kevin W. Lewis

Visualization: Jessica A. Watkins, Nathan T. Stein, Steven G. Banham

Writing – original draft: Jessica A. Watkins, John P. Grotzinger, Dawn Y. Sumner

Writing – review & editing: Jessica A. Watkins, John P. Grotzinger, Sanjeev Gupta, David M. Rubin, Kathryn Stack Morgan, Kenneth S. Edgett, Jens Frydenvang, Kirsten L. Siebach, Michael P. Lamb

by the exhumation of a cratered surface in the 5-km-high central mound of Gale crater, Aeolis Mons (informally known as Mt. Sharp) (Malin & Edgett, 2000).

Early analysis of orbital images and spectra of sedimentary strata exposed in the lower ~350 m of Mt. Sharp strata identified several stratigraphic units of uncertain genesis (Anderson & Bell, 2010; Le Deit et al., 2013; Malin & Edgett, 2000; Milliken et al., 2010; Thomson et al., 2011). Ground mapping by the Curiosity rover showed these rocks to correspond with the fluvial-deltaic Bradbury group plus the overlying-interfingering lacustrine Murray formation of the Mt. Sharp group, both of which were apparently truncated during exhumation and then unconformably overlain by “draping strata” (Grotzinger et al., 2015). These draping, or onlapping, strata were subsequently designated the Stimson formation and interpreted as cross-bedded eolian dune facies (Banham et al., 2018, 2021). The Murray formation exposed in the area of the contact described here shows exclusively deeper lacustrine facies with no evidence for exposure or desiccation (Fedó et al., 2018; Hurowitz et al., 2017; Stack et al., 2019).

Stimson formation sandstone grains display high roundness and sphericity and form sets of cross-bedding up to 1 m in thickness. Bedsets are bounded by sub-horizontal surfaces that can be traced laterally for tens of meters. Much of the cross-bedding is formed as wind-ripple strata (Banham et al., 2018, 2021). The hypothesis that the contact between the Murray and Stimson formations is a significant unconformity, involving denudation of the Mt. Sharp group, predicts local paleotopographic variability along the base of the Stimson formation, in addition to truncation of older strata.

Here we investigate this hypothesis through the systematic, detailed characterization of lateral variations in elevation and geologic expression of the Murray-Stimson contact in the area extending from Amargosa Valley to the Murray Buttes (Figure 1). This corresponds to a stratigraphic level between $-4,460$ m and $-4,370$ m (Figure 1). Rover observations are integrated with larger scale geologic mapping and topographic analysis based on High Resolution Imaging Science Experiment (HiRISE) orbiter data in order to quantitatively reconstruct the topography associated with the contact.

2. Data and Methods

2.1. Rover Image-Based Mapping

Image data were collected by the rover's fixed-focal-length (34 mm M-34 and 100 mm M-100) Mast Camera (Mastcam) during Curiosity's traverse between sols 955 and 1,454 and mosaicked together. Pixel scale varies across and within each mosaic. The M-100 field of view yields a 7.4 cm/pixel scale at 1 km and ~ 150 $\mu\text{m}/\text{pixel}$ at 2.1 m (nearest view to the surface), whereas the M-34 yields a 22 cm/pixel scale at 1 km and 450 $\mu\text{m}/\text{pixel}$ at 2.1 m (Malin et al., 2010).

We mapped the Murray-Stimson contact in selected rover image mosaics based on several distinguishing physical characteristics for each unit: the Stimson formation is a darker-toned (though it can be light-toned when dust covered), resistant, ridge- and talus slope-forming, platy-weathering, medium-grained, cross-bedded, sandstone (Banham et al., 2018, 2021). In contrast, the Murray formation is a lighter-toned, recessive-weathering lithology that does not produce large talus blocks (Edgar et al., 2020; Morris et al., 2016; Stack et al., 2019). The Murray is largely fine-grained mudstone that is thinly to thickly laminated (observable in low light parallel to the surface), with interstratified sandstone lenses, crosscut by abundant Ca-sulfate-filled veins (see Grotzinger et al., 2015 for stratigraphy). The tone difference between these units is similarly evident in their orbital signature, which is lighter for the Murray and darker for the Stimson. The units are also distinguishable based on their geochemistry (see Section 3).

2.2. Mastcam-HiRISE Coordinated Mapping

High-resolution visible wavelength images (up to 0.25 m/pixel) acquired by HiRISE on the Mars Reconnaissance Orbiter spacecraft were also used in this study for detailed photogeologic mapping of the Murray-Stimson contact. Digital terrain models (DTM) (1 km/pixel) produced from HiRISE stereo image pairs (Kirk et al., 2009; McEwen et al., 2007) were used to determine the topography of the paleosurface at the Murray-Stimson contact. HiRISE color image mosaic maps were co-aligned with a high-resolution

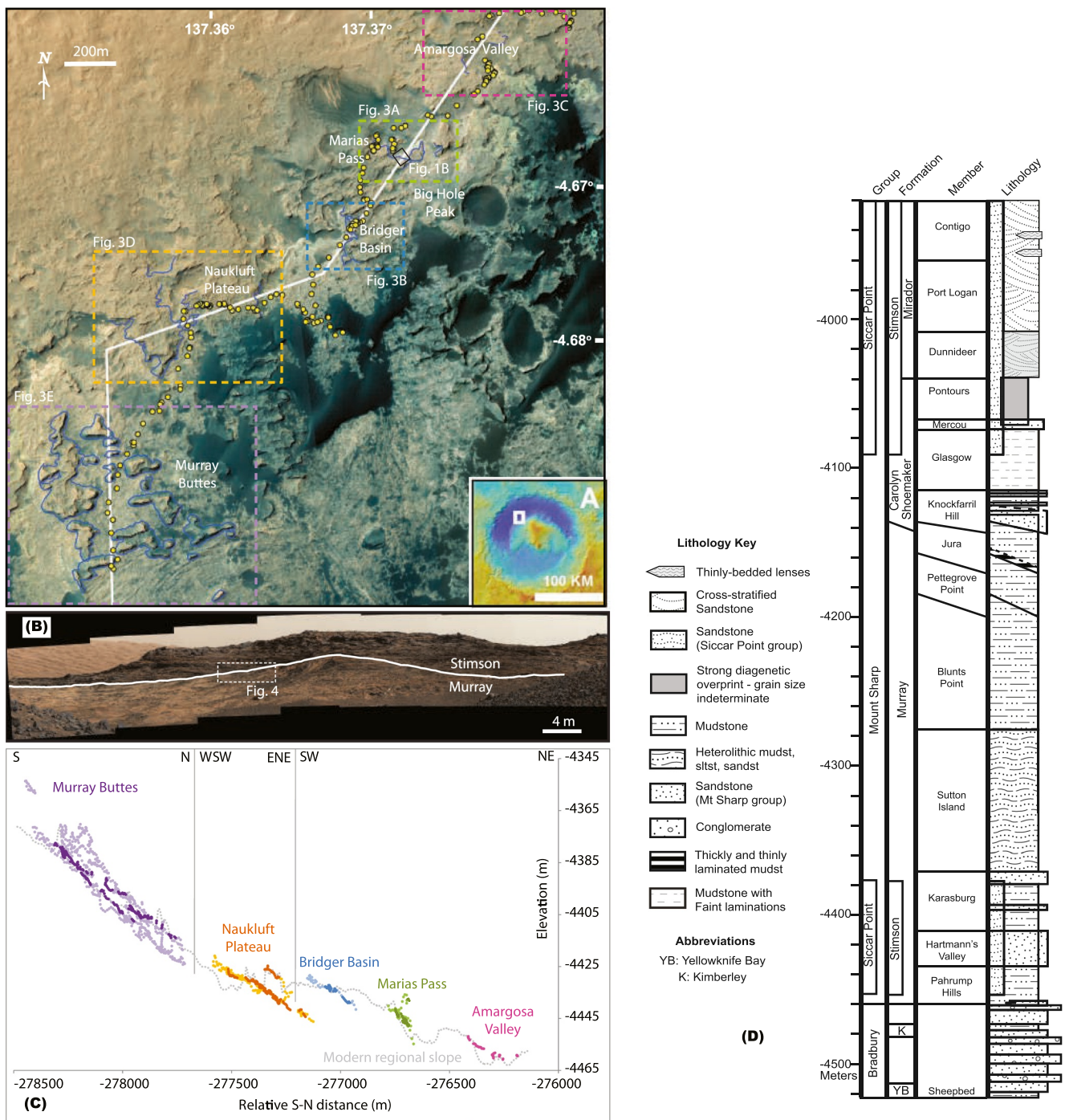


Figure 1. (a) Regional context map of Curiosity rover traverse and sol locations (yellow dots) within lower Mt. Sharp on a High Resolution Imaging Science Experiment (HiRISE) image mosaic; study locations outlined in dashed boxes color-coded by region (also locations of Figure 3), with the mapped Murray-Stimson contact in dark blue. Inset map showing colorized topography of Gale crater from the Mars Orbital Laser Altimeter (MOLA); white box outlines area shown. Small black box denotes location of (b). White line is the representative transect defining modern regional slope in (c). (b) Mastcam mosaic 4,334 (Mastcam-100 lens) acquired on sol 983 with the mapped Murray-Stimson contact at Mt. Stimson in the Marias Pass region. Location of Figure 4 also shown. (c) Plot of elevation versus distance along regional contact in a mostly NE-SW direction (colors correspond to boxed location along the transect in (a); darker shades denote contact mapped in Mastcams; lighter shades, HiRISE), including modern topography along cross-section through mapped areas (white line in (a)). Relative distance is provided by the MOLA topographic coordinate frame. (d) Stratigraphy of the foothills of Mount Sharp showing the location of key units. The Stimson formation has been encountered at two locations; a lower level, described here, exposed from -4,460 m to -4,370 m in elevation and an upper level exposed from -4,090 m to -3,940 m (see Banham et al., 2021).

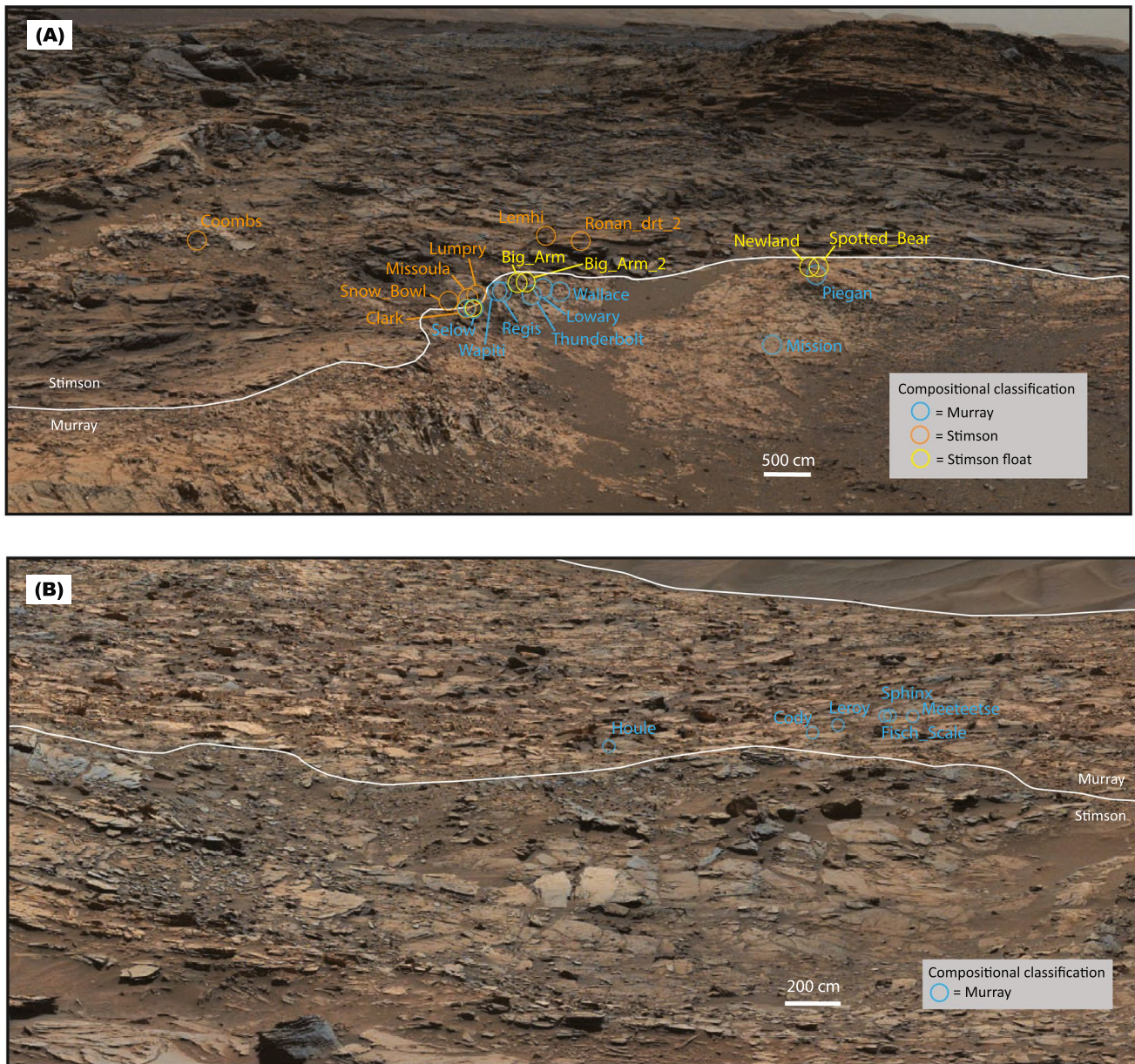


Figure 2. Locations and compositional classification of ChemCam and APXS geochemical targets in stratigraphic context along the independently mapped contact (white line) in (a) Marias Pass (zoom in of Mastcam mosaic mcam04393 using Mastcam-34 lens, acquired on sol 992; see Figure 3a for location) and (b) erosional window in Bridger Basin (zoom in of Mastcam mosaic mcam04918 using Mastcam-100 lens, acquired on sol 1,106; see Figure 3b for location), illustrating correspondence with lithostratigraphy. Chemostratigraphic classification is based on target potassium level as the simplest overall discriminator between units (low K_2O wt% = Stimson; moderate K_2O wt% = Murray) (Frydenvang et al., 2016; Siebach et al., 2017).

DTM mosaic generated for the Mars Science Laboratory (MSL) project from twelve HiRISE stereo pairs that were processed, projected, georeferenced, and mosaicked to create a DTM with 1 m grid spacing, absolute elevations tied to Mars Orbiter Laser Altimeter (MOLA) data, and an expected vertical precision on the order of 0.2–0.3 m (Calef et al., 2013; Golombek et al., 2012; Kirk et al., 2009). A running histogram color stretch that maximizes the dynamic range on $\sim 5,000 \times 5,000$ pixel segments of the image was also applied to highlight distinguishing properties and differentiate between the two formations (Edwards et al., 2011; Fraeman et al., 2016).

Table 1
Variability in Paleorelief Along the Mapped Murray-Stimson Contact, Observed in Mastcam Data and Interpolated From Orbit, by Region (See Figure 1a for Locations; Figure 1c for Elevation Plot, and Figure 3 for Detailed Mapping)

Region	Mastcam		HiRISE (interpolated)	
	Vertical relief (m)	Lateral distance (m)	Total vertical relief (m)	Total lateral distance (m)
Marias Pass	10	250	20	275
Bridger Basin	7	85	13	85
Amargosa Valley	9	180	--	--
Naukluft Plateau	20	560	25	440
Murray Buttes	36	245	71	750

To address the inherent complications related to foreshortening and variable viewing geometry in translating ground-based rover mosaics to plan-view orbital context, we developed a means of systematically coordinating Mastcam and HiRISE image coverage. At each location, the fields of view of selected Mastcam mosaics were systematically plotted onto the HiRISE image using the azimuth and elevation range of each mosaic. Based on integration of the fields of view and topography, viewsheds displaying comprehensive Mastcam mosaic outcrop coverage were computed in ArcGIS. For outcrops with Mastcam data coverage, the contact mapped in the Mastcam images was traced onto the HiRISE image and co-aligned DTM, and topographic profiles along the mapped contact were extracted from the DTM (Nachon et al., 2020). Where no Mastcam data were available, the trace of the contact was interpolated based on unit outcrop expression as observed in HiRISE images, enabling topographic analysis along the regionally continuous contact. This was done based on differences in tone, as mentioned above, as well as texture since the Murray generally appears more uniform and smooth, and the Stimson can be rougher as shown by small shadows.

Once the regional contact was mapped into a shapefile in ArcGIS, natural neighbor 3-D interpolation and trend fit (surface of best fit) of the contact points were then performed with the ArcGIS geoprocessing toolbox. The trend fit was subtracted from this interpolated surface to compute the deviation of elevation from the regional trend of the unconformity along each mapped contact (i.e., the relief), which was overlain on the HiRISE image with a representative color ramp. The choice of natural neighbor interpretation was motivated by its computational simplicity and the desire for the interpolated surface to fall within the range of measured elevations, limiting the likelihood of overestimating eroded thickness.

2.3. Nomenclature

The International Astronomical Union (IAU) determines formal nomenclature for features on Mars. In this manuscript, the following are IAU-designated feature names: Mars, Earth, Gale, Aeolis Mons, and Aeolis Palus. All other place, landform, and investigation target names are informal and were selected by the MSL Science Team during the course of surface operations. Because no International Stratigraphic Code has been established for Mars, all geologic unit names (outcrop, member, formation, group) are also informal. These names originate from a practice established before landing, in which the field site was divided into 1.5×1.5 km quadrangles for the geologic mapping that initially informed the traverse plan. Each quadrangle was named after a geologic formation, group, or supergroup on Earth by the MSL Science Team members responsible for the geologic mapping of a given quadrangle. Names of landforms, targets, and units within those quadrangles were based on other geologic and geographic features that occur in the terrestrial region where the formation, group, or supergroup occurs. Note that some locations, landforms, investigation targets, and geologic units were named posthumously after colleagues connected to Mars exploration or specifically to the MSL mission; in this paper, the features named Murray, for example, honor planetary geoscientist Bruce C. Murray. Others, not discussed here, include the Vera Rubin ridge, named after astronomer Vera Rubin, and the Carolyn Shoemaker formation named after planetary scientist Carolyn Shoemaker.

3. Paleotopographic Mapping

Establishing key physical characteristics for each unit using Mastcam mosaics, we mapped the contact between the darker-toned, medium-grained, platy, cross-bedded Stimson formation sandstone and the lighter-toned, fine-grained, finely laminated, recessively weathered, distinctly veined Murray formation mudstone (Figure 1b). The mapped contact was then traced onto a HiRISE image map and interpolated between Mastcam data coverage to enable topographic analysis along the regionally exposed contact. Geochemical differentiation between

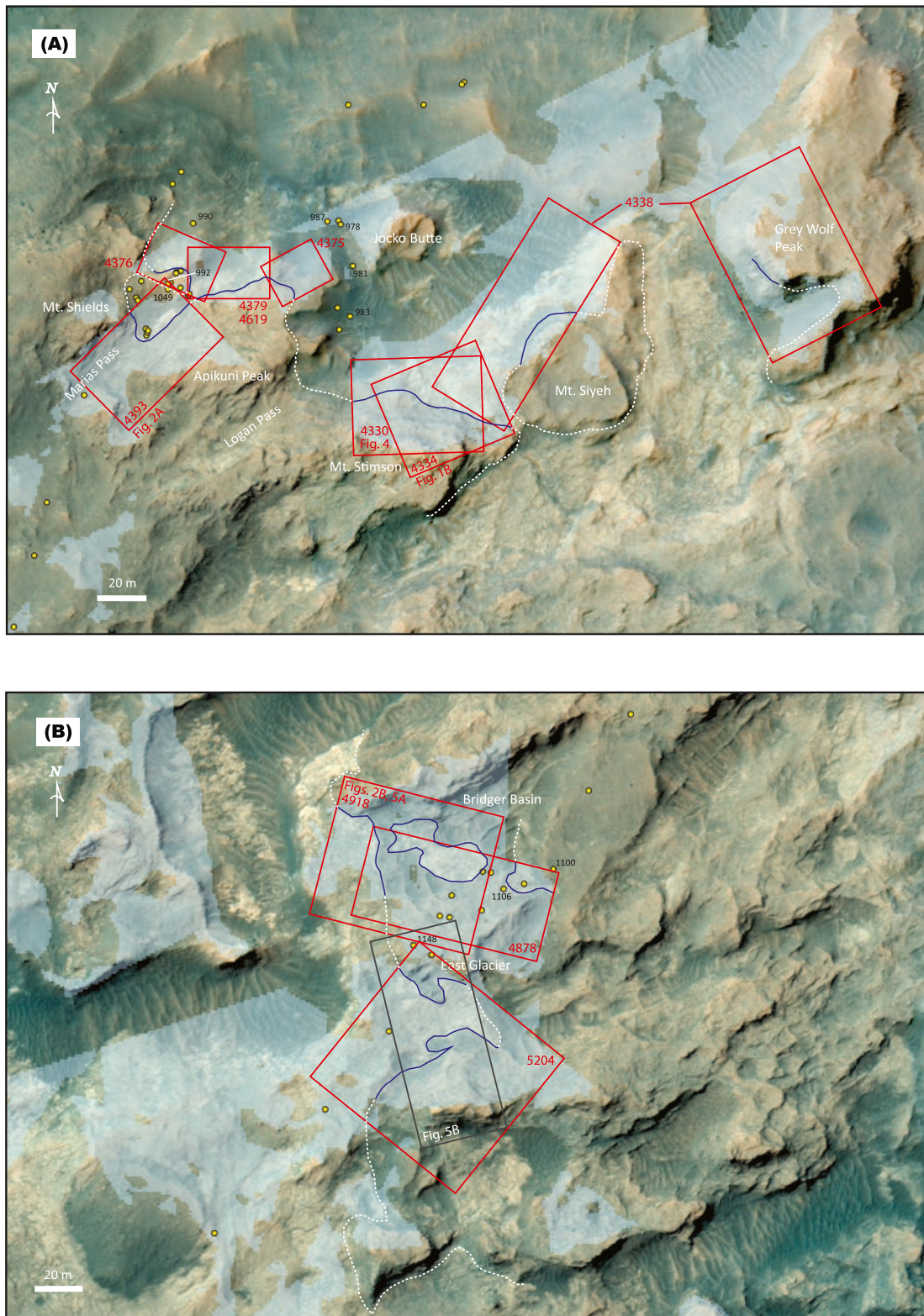


Figure 3.

the Murray and Stimson units in the Marias Pass and Bridger Basin regions (green and blue boxes, respectively, in Figure 1a) was established using laser-induced breakdown spectroscopy (ChemCam) and Alpha-Particle X-Ray Spectrometer (APXS) observations. Classification based on the elemental chemistry of 54 total targets along the contact in these two regions, including float rock, was 100% in agreement with the independent lithostratigraphic classification of these targets based on physical attributes (Figure 2). The principle chemical attribute was (K_2O) , which has a strong dependence on formation (Frydenvang et al., 2016; Siebach et al., 2017). It is worth noting, however, that this chemical separation is not as applicable to other outcrops of the Stimson formation higher up on the slope of Mt. Sharp, for example, in the Greenheugh pediment region (Bedford et al., 2022).

3.1. Local Paleotopographic Variability Along Murray-Stimson Contact

Contact paleorelief was measured where the contact was mapped along Curiosity's traverse path (see Table 1; Figure 1c). In the Marias Pass region, the contact is laterally exposed for 250 m revealing 10 m of local paleorelief, as observed in Mastcam mosaics, and 20 m of total paleorelief along 275 lateral m of the interpolated contact mapped by visual inspection using HiRISE data within the same region (green box in Figures 1a and 1c; Figure 3a). At Mt. Stimson in the Marias Pass region (see Figure 3a for location), progressive updip termination of depositional surfaces within the Stimson along the contact is evident, consistent with onlap of the unconformity. Additionally, ubiquitous Ca-sulfate-filled fractures in the Murray terminate upward at the Murray-Stimson contact, consistent with erosional truncation (Figure 4). Along the southern flank of Mt. Shields, also in the Marias Pass region (see Figure 3a for location), a steep, meter-scale incision is directly observed along the contact, which is onlapped by basal strata of the Stimson sandstone. Centimeter-scale paleorelief is also present along the contact (Edgett et al., 2020; see Figure 2a).

Similar variability in paleorelief is observed in other regions in lower Mt. Sharp (Table 1). At Bridger Basin (blue box in Figures 1a and 1c; Figure 3b), the contact outlines a shallow erosional window through the Stimson that exposes the underlying Murray (Figures 2b and 5a). Also in this region, at East Glacier, gentle paleoridges and paleotroughs of Murray are exposed (Figure 5b). Elsewhere, similar paleolows are infilled by the onlapping Stimson formation. Mapping of the Murray-Stimson contact through Amargosa Valley (pink box in Figures 1a and 1c; Figures 3c and 5c) is complicated by the interfingering of Bradbury group sandstones with the Murray formation mudstones (Grotzinger et al., 2015), substantial sand cover, and isolated mesa exposures in this location, so our analysis here is limited to discontinuous segments.

The Naukluft Plateau region (orange box in Figures 1a and 1c; Figures 3d, 5d and 5e) again exposes abruptly terminated Ca-sulfate veins at the contact on its eastern edge. A second set of veins, very sparsely distributed, crosscuts the Stimson formation, suggesting later fracture and fluid flow events that post-dated the unconformity (Yen et al., 2017). At the Murray Buttes (purple box in Figures 1a and 1c; Figure 3e), the contact is interpreted to largely follow the base of the buttes (Figure 5f).

3.2. Regional-Scale Geometry of Unconformity

The Murray-Stimson contact was mapped laterally to the south for 1.8 km and rises by ~ 140 m, net elevation change (Figure 1c). The mean slope of the unconformity surface is 2.5° based on a linear fit to the contact elevation data, derived from a DTM, and closely follows the modern-day slope of $\sim 1.9^\circ$ based on a linear fit to the same DTM data (Figure 1c). The mapped unconformity surface shows localized but significant deviations from the average 2.5° slope. In particular, low-elevation outliers near Marias Pass and Bridger Basin and high-elevation outliers near Big Hole Peak and the Naukluft Plateau were identified through comparison of the

Figure 3. HiRISE mosaics showing areas viewed in (red boxes) and combined viewsheds of (light blue shading) Mastcams of interest (red annotation indicates Mastcam imaging sequence; e.g., 4,918 = mcam04918), rover traverse by sol (yellow dots; sol numbers on which Mastcams of interest were acquired annotated in black text), the mapped Murray-Stimson stratigraphic contact as seen from rover Mastcam images (dark blue) and interpolated using HiRISE images (white dashed) for the following Curiosity rover study areas: (a) Marias Pass (see green box in Figure 1a for location; locations of Figures 1b, 2a and 4 also shown), (b) Bridger Basin (see blue box in Figure 1a for location; locations of Figures 2b, 5a and 5b also shown), (c) Amargosa Valley (see pink box in Figure 1a for location; location of Figure 5c also shown), (d) Naukluft Plateau (see orange box in Figure 1a for location; locations of Figures 5d and 5e also shown), and (e) Murray Buttes (see purple box in Figure 1a for location; location of Figure 5f also shown).

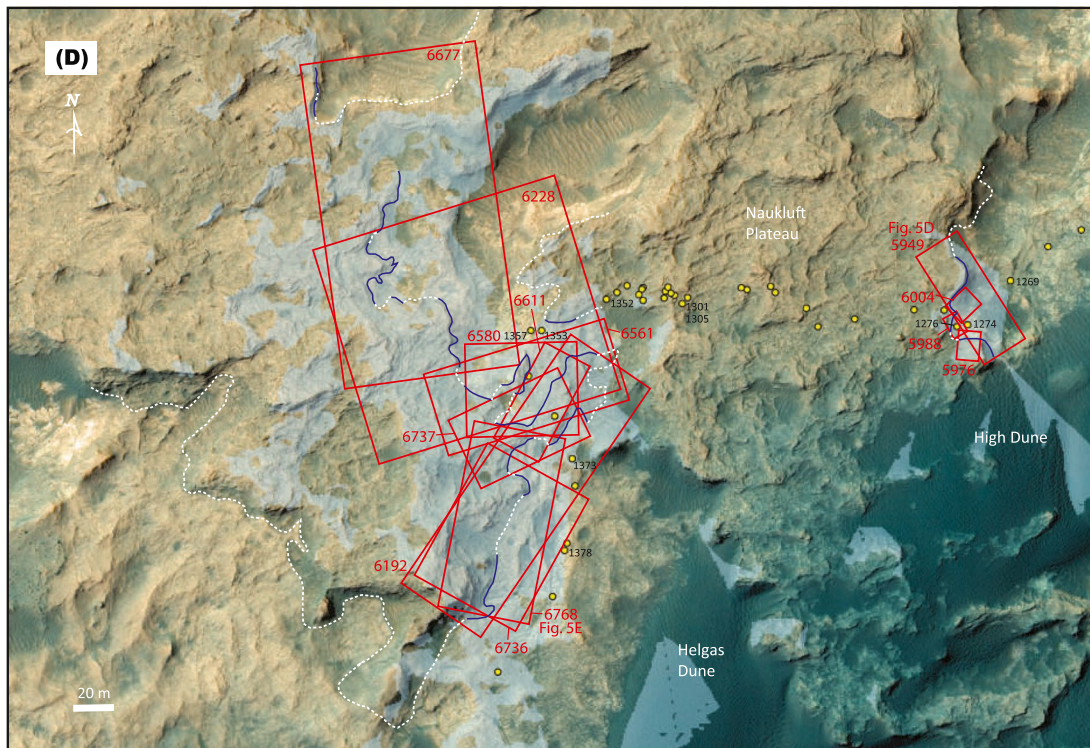
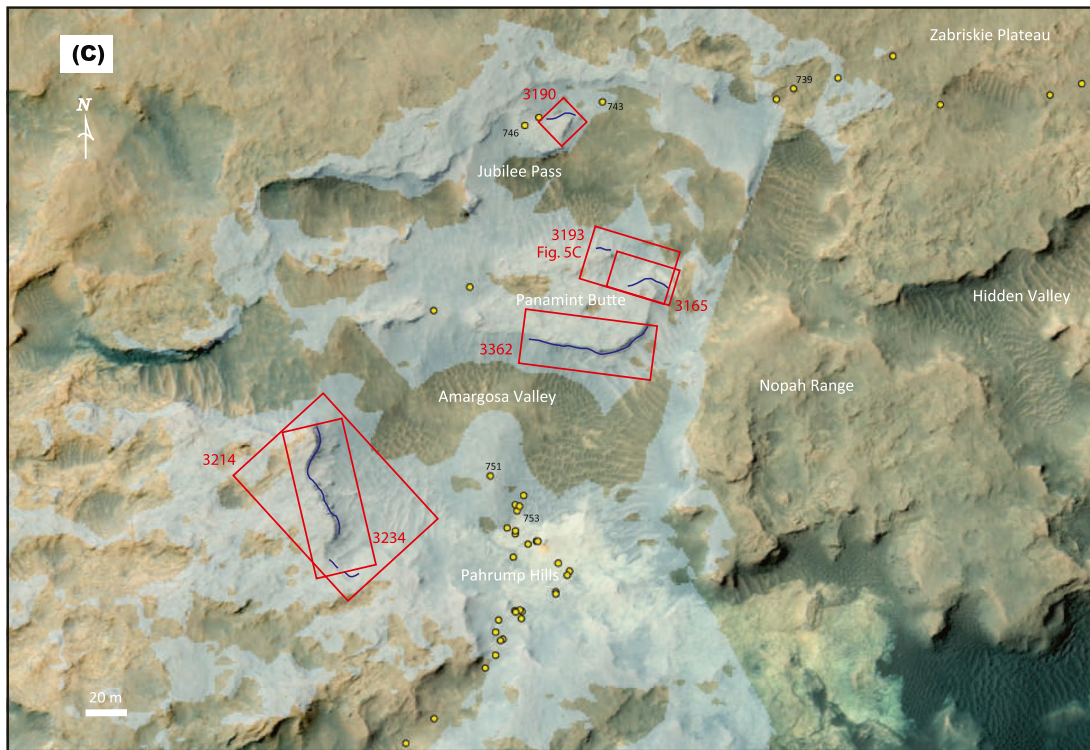


Figure 3. (Continued)

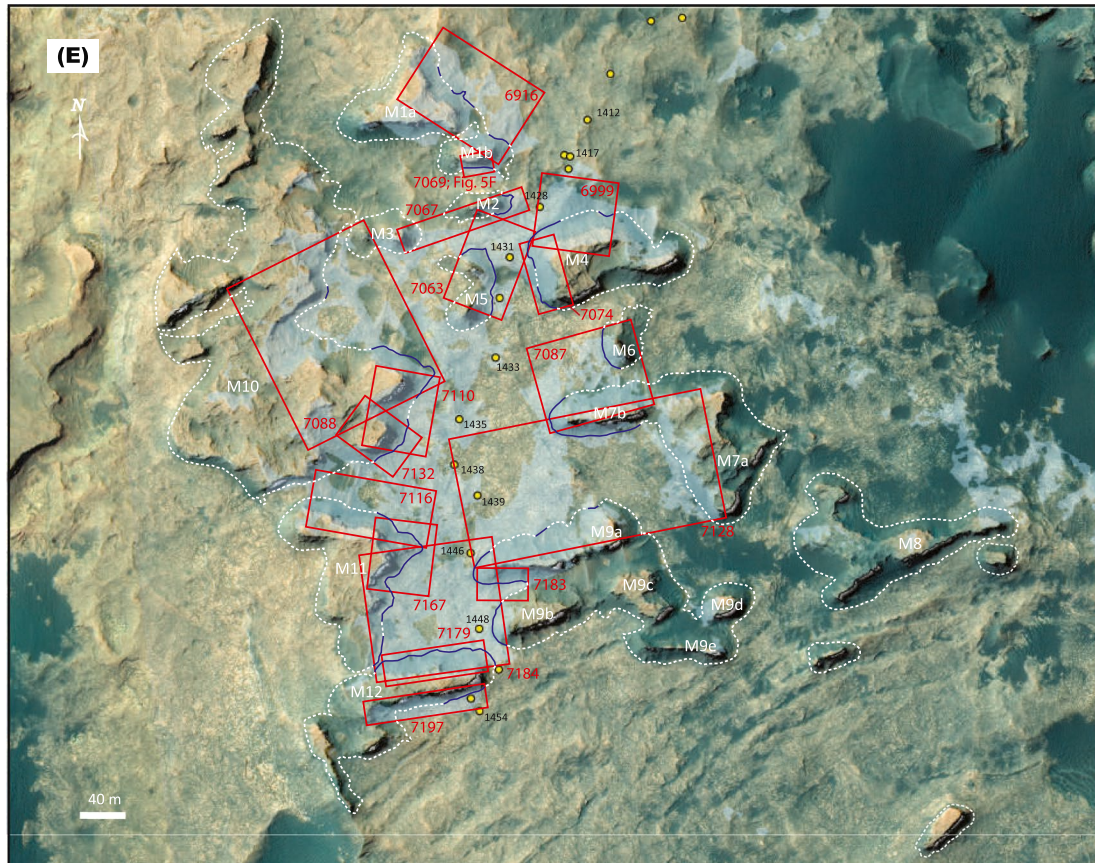


Figure 3. (Continued)

interpolated 3-D contact with both the surface of best fit through the mapped contacts (Figure 6) and a representative surface within the regional DTM (Figure 7).

This mapping is the first of its kind at Gale crater. Previous studies (Banham et al., 2018; Grotzinger et al., 2015) proposed the unconformity based on the sharp juxtaposition of the eolian Stimson sandstone above the lacustrine Murray mudstone. However, this could represent a simple lowstand in lake level followed by the emplacement of a wedge of eolian wind-blown sand without requiring a significant gap in time (*sensu* Carroll & Bohacs, 1999) in contrast to the unconformity hypothesis developed here. The latter requires demonstration of significant erosion at a local as well as a more regional scale. Most recently, the Stimson formation was correlated to rocks further upslope, several kilometers to the south. Here, the same abrupt truncation surface can be observed at the contact with the “Greenheugh Pediment,” which marks the same unconformity, indicating it has regional extent (Banham et al., 2021; Bryk et al., 2020).

4. Discussion

On Earth, regional unconformities may be identified based on stratal geometries (e.g., Vail et al., 1977); erosional truncation and onlap are diagnostic expressions. The observed onlap of the Murray-Stimson contact, coupled with significant variability in paleorelief, truncation of diagenetic veins, and reworking of older strata and their veins to form clasts deposited along surface (Edgett et al., 2020; Newsom et al., 2016), all support the interpretation of an erosional unconformity at the base of the Stimson formation. Local, rover-based observations of the meter-scale incision along the unconformity surface support the regional identification of an undulating, erosional paleosurface. Eolian facies within basal Stimson strata implicate eolian abrasion as the likely mechanism of erosion, particularly because fluvial deposits such as channel sandstones or conglomerates are absent in

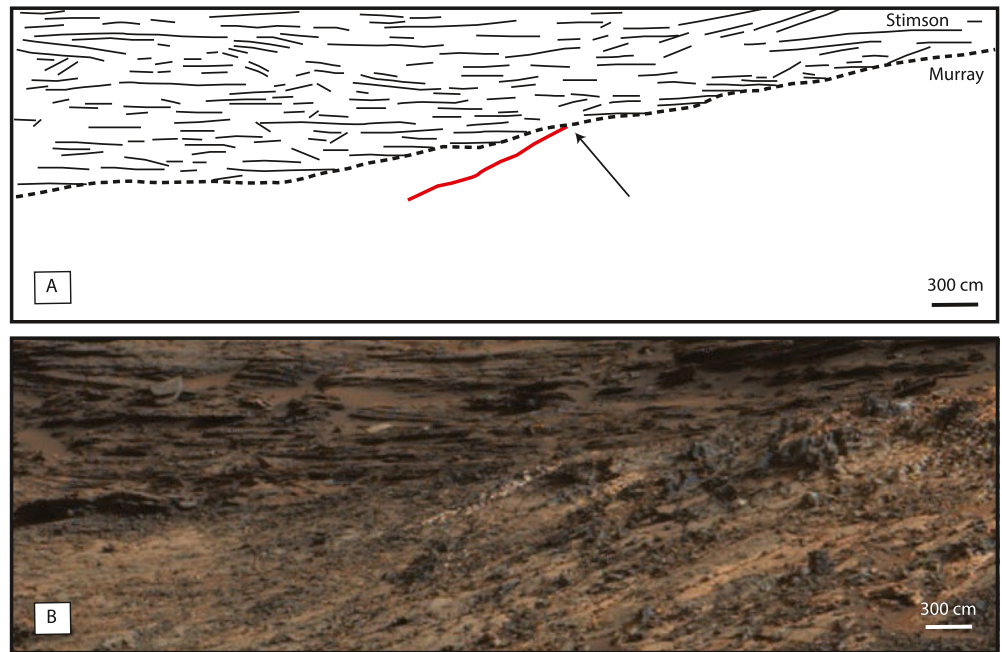


Figure 4. (a) Map of features in the zoom in of Mastcam mosaic mecam04330 (Mastcam 100 lens) acquired on sol 980 showing a prominent Ca-sulfate-filled vein (red) in the Murray formation, truncation (denoted with arrow) along the Murray-Stimson contact (black dashed line), and bedding planes (black solid lines), which display onlap along the unconformity (see Figure 1b for location). (b) Unmarked mosaic in (a).

the mapped low points of the paleosurface (Newsom et al., 2016; Edgett et al., 2020). This matches experimental and theoretical predictions (Day et al., 2016) that erosion of older Gale strata could have formed Mt. Sharp by eolian-driven exhumation. Outlier deviations from the regional contact dip may represent local effects such as buried impact craters, accentuated wind-scoured topography, or even fluvial incised valleys that were not observed by Curiosity.

The orientation of the unconformity provides a constraint on the erosional process that likely contributed to the present-day morphology of Gale's central mound. The northward-sloping paleosurface is closely aligned with the modern day slope, suggesting that erosional processes in the past may have been similar to those operating on more recent timescales. Since more recent erosion at Gale appears to be governed by eolian processes (Bridges et al., 2014; Farley et al., 2014), it seems likely that this was also true in the deep past. Recent experimental and numerical modeling studies of Gale morphologic analogs have shown that topographically focused wind circulation patterns favor the excavation of a central mound, given an initially thick sequence of layered sedimentary crater fill (Day et al., 2016). In these studies, the fill is eroded by the wind in a fashion that produces a central mound consistent with the form of Mt. Sharp. In particular, the region of the crater that is being explored by Curiosity is predicted to be excavated, producing a depression occupied by the Gale northern crater moat (Aeolis Palus) and an exhumation surface at the position of Curiosity's traverse path with a northward-dipping slope. At a more global scale, eolian-driven exhumation also accounts for the formation of intracrater mounds (Bennett & Bell, 2016; Grotzinger & Milliken, 2012; Malin & Edgett, 2000).

Crater age estimates constrain the interval of deposition of Gale's initial fill (Bradbury group, Mt. Sharp group, and any older subsurface strata) as well as the interval of erosion and exhumation to ~500 My, spanning from 3.8 to 3.6 to 3.3–3.1 Ga (Grant et al., 2014; Grotzinger et al., 2015). Unfortunately, the absolute age of the Stimson formation is not known due to its limited areal exposure for crater counting. Therefore, the post-exhumation onlap by the Stimson formation could have occurred within and/or after this time interval. Either scenario indicates that the unconformity could have spanned hundreds of millions of

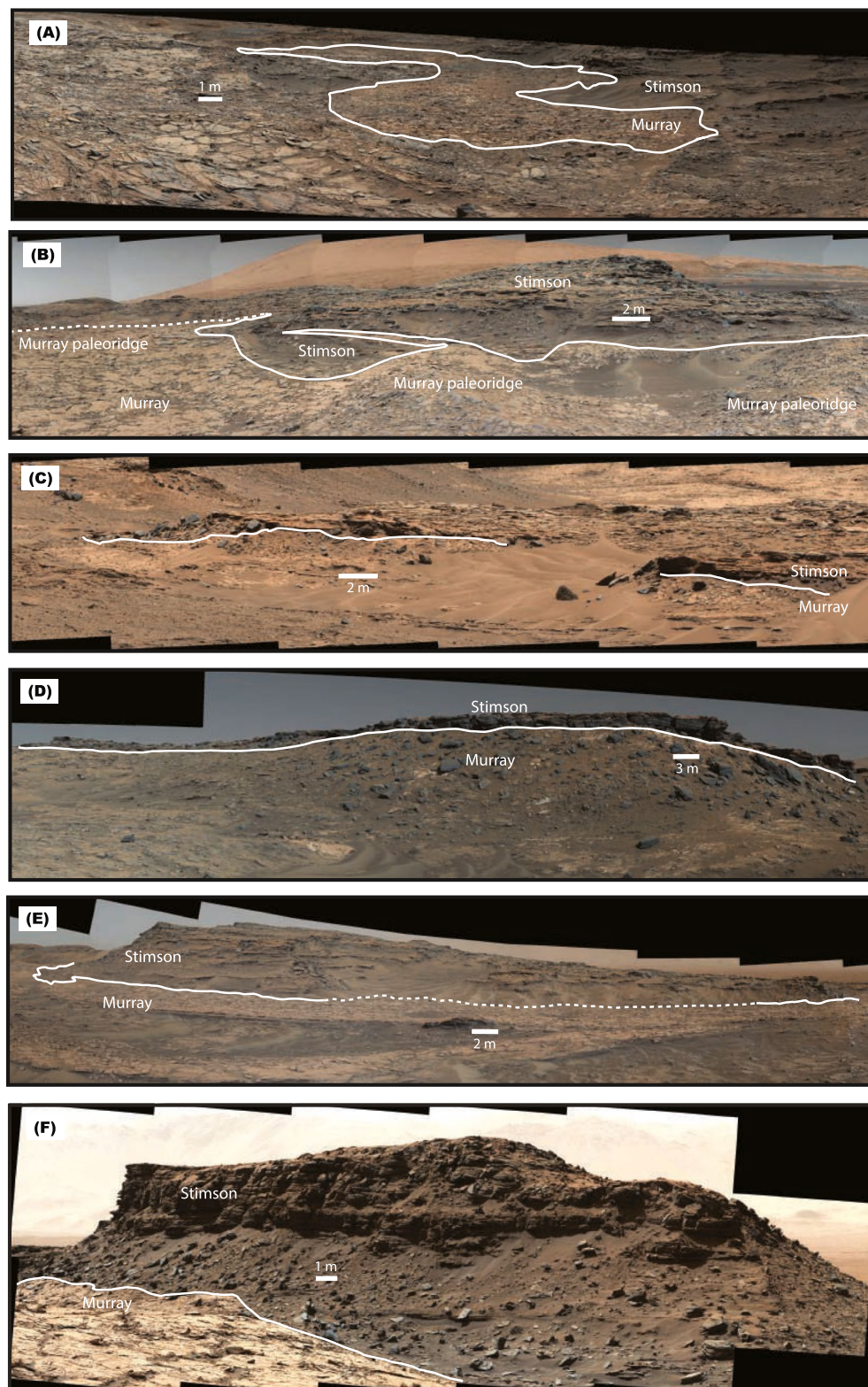


Figure 5. Key Mastcam mosaics with the Murray-Stimson contact mapped (solid white line; dashed, location uncertain due to obscuration) at the following sites: (a) Bridger Basin (Mastcam mosaic mcam04918, Mastcam 100 lens, acquired on sol 1,106; see Figure 3b for location), (b) East Glacier (mcam05216, Mastcam 34 lens, acquired on sol 1,154; see Figure 3b for location), (c) Amargosa Valley (mcam03193, Mastcam 34 lens, acquired on sol 744; see Figure 3c for location), (d) eastern Naukluft Plateau (mcam05949, Mastcam 100 lens, acquired on sol 1,272; see Figure 3d for location), (e) western Naukluft Plateau (mcam06768, Mastcam 34 lens, acquired on sol 1,381; see Figure 3d for location), and (f) Murray Buttes (mcam07069, Mastcam 100 lens, acquired on sol 1,429; see Figure 3e for location).

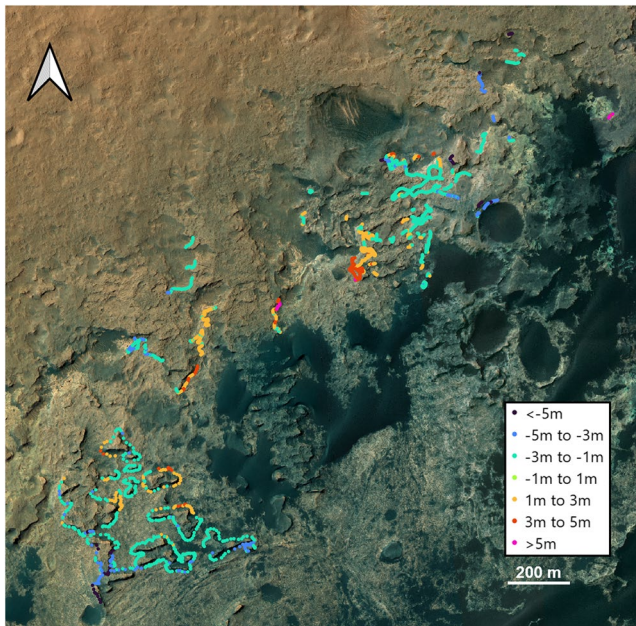


Figure 6. Deviation in elevation (in meters) of the interpolated regional Murray-Stimson contact surface from surface of best fit through the contact plotted on mosaic of HiRISE images. Warm colors denote positive deviation; cool colors, negative. Note the variability in paleorelief and outliers along the contact.

years. The shift from the dominantly lacustrine environment represented by the Murray formation (Edgar et al., 2020; Fedo et al., 2018; Grotzinger et al., 2015) to the dry, eolian environment of the Stimson formation (Banham et al., 2018, 2021) could be a record of the transition of Mars' global environment from wet to predominantly dry, as suggested by orbiter observations of the stratigraphic record (Grotzinger & Milliken, 2012; Milliken et al., 2010).

A proposed evolutionary sequence that accounts for the stratigraphy and morphology of the lower Mt. Sharp group observed in this study (Figure 8) involves: (a) deposition of the Mt. Sharp group, including Murray lacustrine sediments during a period of wet climate, followed by their burial and lithification (Edgar et al., 2020; Fedo et al., 2018; Grotzinger et al., 2015), (b) the subsequent deposition of overlying Mt. Sharp group sediments (Grotzinger et al., 2015), (c) transition to dry climate accompanied by wind erosion and exhumation of the buried Mt. Sharp group, including the Murray formation, (d) a shift of conditions in the northern crater from net erosion to net sediment accumulation to deposit the Stimson eolian sediments (Banham et al., 2018, 2021) that mantled the unconformity paleoslope (Bryk et al., 2020), (e) burial and cementation of Stimson strata (Banham et al., 2018, 2021; Frydenvang et al., 2016), and (f) return to the conditions of net erosion, which exhumed and eroded the Stimson formation to create the remnant patches that are exposed across the modern surface (Edgett et al., 2020).

The proposed events outlined above highlight the dynamic environmental history of Gale crater, recorded by both the strata and their bounding unconformable surfaces. In 1909, Eliot Blackwelder noted the significance of unconformities on Earth (Blackwelder, 1909) and recognized that understanding their structure, and the partitioning of time, could aid in reconstructing past events—a principle subsequently extended by Wheeler (1964), Sloss (1963), and Vail et al. (1977). With a similar purpose we suggest that the north-sloping geometry of the base-Stimson unconformity at Gale crater may record uniquely martian processes, by which long-lived events of eolian denudation, controlled by the flow of air in the absence of tectonic forces, have become embedded within the rock record. Furthermore, that the modern slope so closely follows the ancient slope implies a certain uniformity of process over the gulf of martian geologic time.

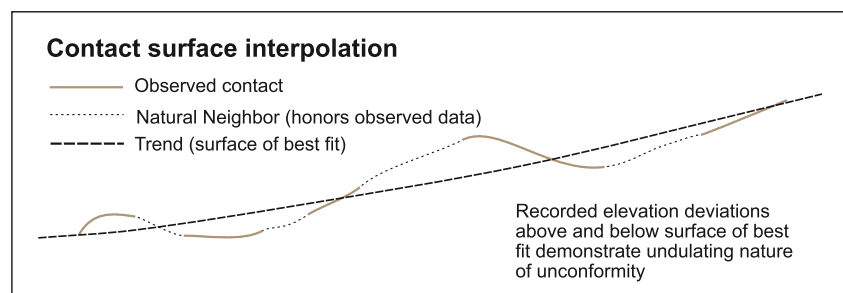


Figure 7. Methods for interpolating the contact surface, showing natural neighbor interpolation and trend fit.

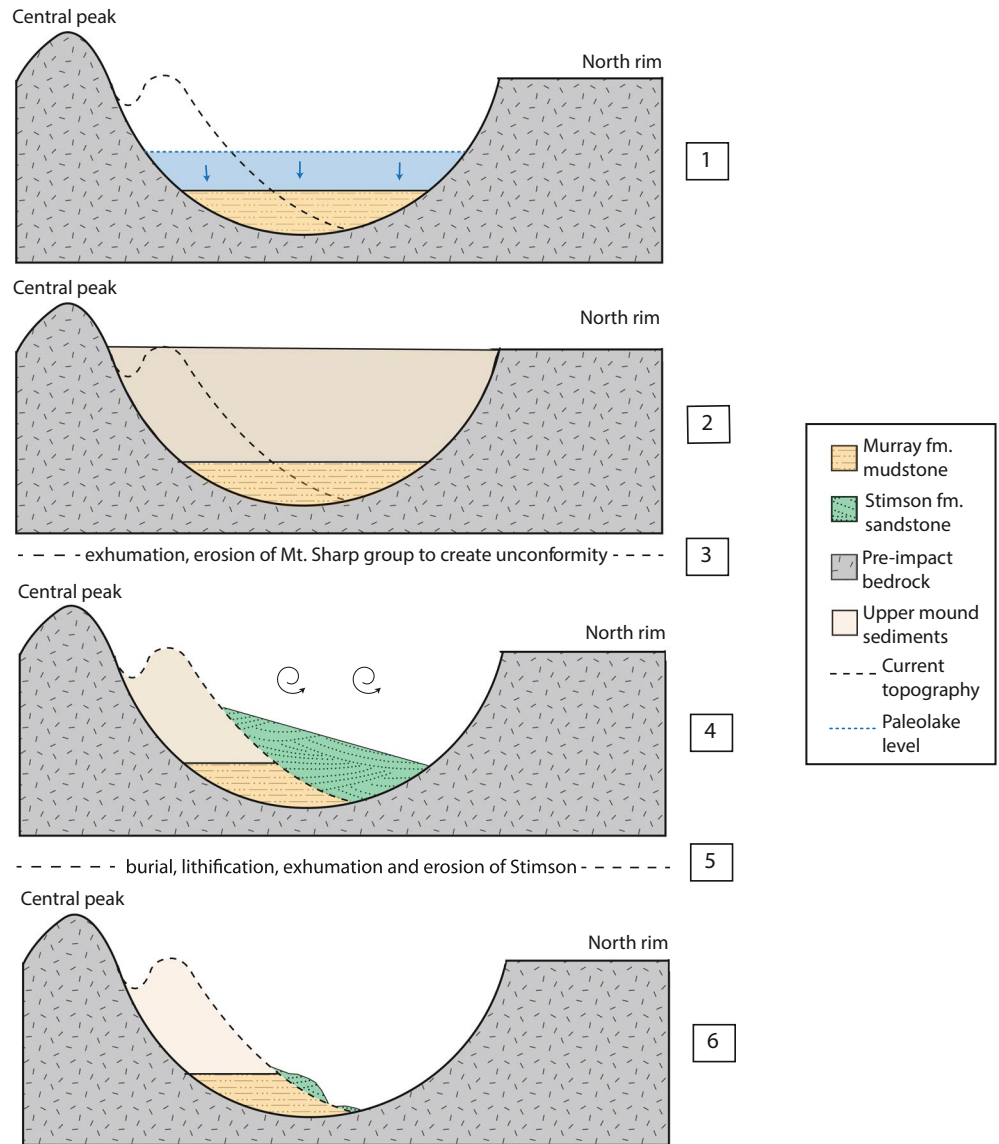


Figure 8. Schematic cartoon of the proposed lower Mt. Sharp evolutionary sequence: (a) Murray formation deposition, burial, and lithification associated with a lake, (b) depositional, burial, and lithification of overlying Mt. Sharp group sediments, (c) erosion and exhumation of Mt. Sharp group to produce an unconformity, (d) Stimson formation deposition against erosional surface (unconformity) slope, (e) burial, lithification, exhumation, and erosion of Stimson, and (f) present-day surface with preserved Stimson remnants.

Acknowledgments

We thank the scientists and engineers of the Mars Science Laboratory mission and Mars Reconnaissance Orbiter teams for their work in obtaining the observations analyzed in this study and for their contributions that have made the Curiosity mission a success. All raw data products supporting the conclusions of this work can be obtained from the NASA Planetary Data System (PDS). All MSL Mastcam images (Malin, 2013) can be downloaded from the Curiosity (MSL) Analyst's Notebook (<https://an.rsl.wustl.edu/msl/mslbrowser/an3.aspx>), where they are searchable by ID and Sol listed in the figure captions. Funding was provided by NASA.

Data Availability Statement

All HiRISE images (McEwen, 2007, 2009) can be downloaded from the PDS Geosciences Node Mars Orbital Data Explorer (<https://ode.rsl.wustl.edu/mars/>). Archived data are accessible here: <https://data.caltech.edu/records/20101>, see Watkins et al. (2022).

References

- Anderson, R. B., & Bell, J. F., III. (2010). Geologic mapping and characterization of Gale Crater and implications for its potential as a Mars Science Laboratory landing site. *MARS*, 5, 76–128. <https://doi.org/10.1555/mars.2010.0004>
- Banham, S. G., Gupta, S., Rubin, D. M., Edgett, K. S., Van Beek, J., Watkins, J. A., et al. (2021). Rock record of complex aeolian bedforms in a Hesperian desert landscape: The Stimson formation as exposed in the Murray Buttes, Gale crater, Mars. *Journal of Geophysical Research: Planets*, 126(4). <https://doi.org/10.1029/2020JE006554>

- Banham, S. G., Gupta, S., Rubin, D. M., Watkins, J. A., Sumner, D., Edgett, K. S., et al. (2018). Ancient Martian aeolian processes and paleomorphology reconstructed from the Stimson formation on the lower slope of Aeolis Mons, Gale crater, Mars. *Sedimentology*, *65*(4), 993–1042. <https://doi.org/10.1111/sed.12469>
- Bedford, C. C., Banham, S. G., Bridges, J. C., Forni, O., Cousin, A., Bowden, D., et al. (2022). An insight into ancient aeolian processes and post-Noachian aqueous alteration in Gale crater, Mars, using ChemCam geochemical data from the Greenheugh capping unit. *Journal of Geophysical Research: Planets*. <https://doi.org/10.1029/2021je007100>
- Bennett, K. A., & Bell, J. F., III. (2016). A global survey of martian central mounds: Central mounds as remnants of previously more extensive large-scale sedimentary deposits. *Icarus*, *264*, 331–341. <https://doi.org/10.1016/j.icarus.2015.09.041>
- Blackwelder, E. (1909). The valuation of unconformities. *The Journal of Geology*, *17*(3), 289–299. <https://doi.org/10.1086/621610>
- Bridges, N. T., Calef, F. J., Hallet, B., Herkenhoff, K. E., Lanza, N. L., Le Mouelic, S., et al. (2014). The rock abrasion record at Gale crater: Mars Science Laboratory results from Bradbury landing to rocknest. *Journal of Geophysical Research: Planets*, *119*(6), 1374–1389. <https://doi.org/10.1002/2013JE004579>
- Bryk, A. B., Dietrich, W. E., Lamb, M. P., Grotzinger, J. P., Vasavada, A. R., Stack, K. M., et al. (2020). *New evidence for climate and erosion history in Gale crater, Mars, from Curiosity's ascent onto the Greenheugh pediment*. AGU 2020 Fall meeting.
- Calef, F. J., III, Dietrich, W. E., Edgar, L., Farmer, J., Fraeman, A., Grotzinger, J., et al. (2013). Geologic mapping of the Mars Science Laboratory landing ellipse. *Lunar and Planetary Science Conference*, *44*, 2511.
- Carroll, A., & Bohacs, K. (1999). Stratigraphic classification of ancient lakes: Balancing tectonic and climatic controls. *Geology*, *27*(2), 99–102. <https://doi.org/10.1130/0091-7613>
- Day, M., Anderson, W., Kocurek, G., & Mohrig, D. (2016). Carving intracrater layered deposits with wind on Mars. *Geophysical Research Letters*, *43*(6), 2473–2479. <https://doi.org/10.1002/2016GL068011>
- Edgar, L. A., Fedo, C. M., Gupta, S., Banham, S. G., Fraeman, A. A., Grotzinger, J. P., et al. (2020). A lacustrine paleoenvironment recorded at Vera Rubin ridge, Gale crater: Overview of the sedimentology and stratigraphy observed by the Mars Science Laboratory curiosity rover. *Journal of Geophysical Research: Planets*, *125*(3). <https://doi.org/10.1029/2019JE006307>
- Edgett, K. S., Banham, S. G., Bennett, K., Edgar, L. A., Edwards, C. S., Fedo, C. M., et al. (2020). Extraformational sediment recycling on Mars. *Geosphere*, *16*(6), 1508–1537. <https://doi.org/10.1130/GES02244.1>
- Edwards, C. S., Nowicki, K. J., Christensen, P. R., Hill, J., Gorelick, N., & Murray, K. (2011). Mosaicking of global planetary image datasets: 1. Techniques and data processing for thermal emission imaging system (THEMIS) multi-spectral data. *Journal of Geophysical Research*, *116*(E10), E10008. <https://doi.org/10.1029/2010JE003755>
- Eigenbrode, J. L., Summons, R. E., Steele, A., Freissinet, C., Millan, M., Sutter, B., et al. (2018). Organic matter preserved in 3-billion-year-old mudstones at Gale crater, Mars. *Science*, *360*(6393), 1096–1101. <https://doi.org/10.1126/science.aas9185>
- Farley, K. A., Malespin, C., Mahaffy, P., Grotzinger, J. P., Vasconcelos, P. M., Milliken, R. E., et al. (2014). In situ radiometric and exposure age dating of the Martian surface. *Science*, *343*(6169). <https://doi.org/10.1126/science.1247166>
- Fedo, C. M., Grotzinger, J. P., Gupta, S., Fraeman, A., Edgar, L., Edgett, K., & Vasavada, A. R. (2018). Sedimentology and stratigraphy of the Murray formation, Gale crater, Mars. *Lunar and Planetary Science Conference*, *49*, 2973. Lunar and Planetary Institute Contribution 2078.
- Fraeman, A. A., Ehlmann, B., Arvidson, R. A., Grotzinger, J. P., Milliken, R., Milliken, R. E., et al. (2016). The stratigraphy and evolution of lower Mt. Sharp from spectral, morphological, and thermophysical orbital datasets. *Journal of Geophysical Research: Planets*, *121*(9), 1713–1736. <https://doi.org/10.1002/2016JE005095>
- Freissinet, C., Glavin, D. P., Mahaffy, P. R., Miller, K. E., Eigenbrode, J. L., Summons, R. E., et al. (2015). Organic molecules in the sheepbed mudstone, Gale crater, Mars. *Journal of Geophysical Research: Planets*, *120*(3), 495–514. <https://doi.org/10.1002/2014JE004737>
- Frydenvang, J., Hurowitz, J. A., Grotzinger, J. P., Wiens, R. C., Newsom, H. E., Bridges, J., et al. (2016). Discovery of silica-rich lacustrine and eolian sedimentary rocks in Gale crater, Mars. *Lunar and Planetary Science Conference*, *47*, 2349.
- Golombek, M. P., Grant, J., Kipp, D., Vasavada, A., Kirk, R., Fergason, R., et al. (2012). Selection of the Mars Science Laboratory landing site. *Space Science Reviews*, *170*(1–4), 641–737. <https://doi.org/10.1007/s11214-012-9916-y>
- Grant, J. A., Wilson, S. A., Mangold, N., Calef, F., III, & Grotzinger, J. P. (2014). The timing of alluvial activity in Gale crater, Mars. *Geophysical Research Letters*, *41*(4), 1142–1149. <https://doi.org/10.1002/2013gl058909>
- Grotzinger, J. P., Gupta, S., Malin, M. C., Rubin, D. M., Schieber, J., Siebach, K., et al. (2015). Deposition, exhumation, and paleoclimate of an ancient lake deposit, Gale crater, Mars. *Science*, *350*(6257). <https://doi.org/10.1126/science.aac7575>
- Grotzinger, J. P., & Milliken, R. E. (2012). The sedimentary rock record of Mars: Distribution, origins, and global stratigraphy. *Sedimentary Geology of Mars*, *102*, 1–48. <https://doi.org/10.2110/pec.12.102.0001>
- Hurowitz, J. A., Grotzinger, J. P., Fischer, W., McLennan, S. M., Milliken, R., Stein, N., et al. (2017). Redox stratification of an ancient lake in Gale crater, Mars. *Science*, *356*(6341). <https://doi.org/10.1126/science.aah6849>
- Kirk, R. L., Howington-Kraus, E., Rosiek, M. R., Anderson, J. A., Archinal, B. A., Becker, K. J., et al. (2009). Ultrahigh resolution topographic mapping of Mars with MRO HiRISE stereo images: Meter-scale slopes of candidate Phoenix landing sites. *Journal of Geophysical Research*, *113*, E00A24. <https://doi.org/10.1029/2007JE003000>
- Le Deit, L. L., Hauber, E., Fueten, F., Pondrelli, M., Rossi, A. P., & Jaumann, R. (2013). Sequence of infilling events in Gale Crater, Mars: Results from morphology, stratigraphy, and mineralogy. *Journal of Geophysical Research: Planets*, *118*(12), 2439–2473. <https://doi.org/10.1002/2012JE004322>
- Malin, M. (2013). MSL Mars mast Camera RDR V1.0, NASA planetary data system. *MSL-M-MASTCAM-4-RDR-IMG-V1.0*. <https://doi.org/10.17189/1520328>
- Malin, M. C., Caplinger, M. A., Edgett, K. S., Ghaemi, F. T., Ravine, M. A., Schaffner, J. A., et al. (2010). The Mars Science Laboratory (MSL) mast-mounted cameras (Mastcams) flight instruments. *Lunar and Planetary Science Conference*, *41*, 1123.
- Malin, M. C., & Edgett, K. S. (2000). Sedimentary rocks of early Mars. *Science*, *290*(5498), 1927–1937. <https://doi.org/10.1126/science.290.5498.1927>
- McEwen, A. (2007). Mars reconnaissance orbiter high resolution imaging science experiment, reduced data record, MRO-M-HIRISE-3-RDR-V1.1. *NASA Planetary Data System*. <https://doi.org/10.17189/1520303>
- McEwen, A. (2009). Mars reconnaissance orbiter high resolution imaging science experiment, digital terrain model, MRO-M-HIRISE-5-DTM-V1.0. *NASA Planetary Data System*. <https://doi.org/10.17189/1520227>
- McEwen, A. S., Eliason, E. M., Bergstrom, J. W., Bridges, N. T., Hansen, C. J., Delamere, W. A., et al. (2007). Mars reconnaissance orbiter's high resolution imaging science experiment (HiRISE). *Journal of Geophysical Research*, *115*(E5), E05S02. <https://doi.org/10.1029/2005JE002605>
- Milliken, R. E., Grotzinger, J. P., & Thomson, B. J. (2010). Paleoclimate of Mars as captured by the stratigraphic record in Gale Crater. *Geophysical Research Letters*, *37*(4). <https://doi.org/10.1029/2009GL041870>

- Morris, R. V., Vaniman, D. T., Blake, D. F., Gellert, R., Chipera, S. J., Rampe, E. B., et al. (2016). Silicic volcanism on Mars evidenced by tridymite in high-SiO₂ sedimentary rock at Gale crater. *Proceedings of the National Academy of Sciences*, 113(26), 7071–7076. <https://doi.org/10.1073/pnas.1607098113>
- Nachon, M., Borges, S., Ewing, R., Rivera-Hernandez, F., Stein, N., & Van Beek, J. (2020). Coupling Mars ground and orbital views: Generate viewsheds of Mastcam images from the curiosity rover, using ArcGIS® and public datasets. *Earth and Space Science*. <https://doi.org/10.1029/2020EA001247>
- Newsom, H. E., Belgacem, I., Jackson, R., Ha, B., Vaci, Z., Wiens, R., et al. (2016). The materials at an unconformity between the Murray and Stimson formations at Marias pass, Gale crater, Mars. *Lunar and Planetary Science Conference*, 47, 2397.
- Sadler, P. M. (1981). Sediment accumulation rates and the completeness of stratigraphic sections. *The Journal of Geology*, 89(2), 569–584. <https://doi.org/10.1086/628623>
- Siebach, K. L., Baker, M. B., Grotzinger, J. P., McLennan, S. M., Gellert, R., Thompson, L., & Hurowitz, J. (2017). Sorting out compositional trends in sedimentary rocks of the Bradbury group (Aeolis Palus), Gale Crater, Mars. *Journal of Geophysical Research: Planets*, 122(2), 295–328. <https://doi.org/10.1002/2016JE005195>
- Sloss, L. L. (1963). Sequences in the cratonic interior of North America. *The Geological Society of America Bulletin*, 74(2), 93–114. [https://doi.org/10.1130/0016-7606\(1963\)74\(93:sticio\)2.0.co;2](https://doi.org/10.1130/0016-7606(1963)74(93:sticio)2.0.co;2)
- Stack, K. M., Grotzinger, J. P., Lamb, M. P., Gupta, S., Rubin, D. M., Kah, L. C., et al. (2019). Evidence for plunging river plume deposits in the Pahrump Hills member of the Murray formation, Gale crater, Mars. *Sedimentology*, 66(5), 1768–1802. <https://doi.org/10.1111/sed.12555>
- Thomson, B. J., Bridges, N., Milliken, R., Baldrige, A., Hook, S., Crowley, J., et al. (2011). Constraints on the origin and evolution of the layered mound in Gale Crater, Mars using Mars Reconnaissance Orbiter data. *Icarus*, 214(2), 413–432. <https://doi.org/10.1016/j.icarus.2011.05.002>
- Vail, P. R., Todd, R. G., & Sangree, J. B. (1977). Seismic stratigraphy and global changes of sea level: Part 5. Chronostratigraphic significance of seismic reflections: Section 2. Application of seismic reflection configuration to stratigraphic interpretation. In *Seismic stratigraphy- applications to hydrocarbon exploration* (pp. 99–116). American Association of Petroleum Geologists.
- Watkins, J., Gupta, S., Rubin, D. M., Watkins, J. A., Sumner, D. Y., Edgett, K. S., et al. (2022). Shapefile containing a trace of the Murray-Stimson contact in Gale crater, Mars based on images from the Mars Science Laboratory (MSL) rover and HiRISE [Dataset]. CaltechDATA. <https://doi.org/10.22002/D1.20101>
- Wheeler, H. E. (1964). Baselevel, lithosphere surface, and time-stratigraphy. *The Geological Society of America Bulletin*, 75(7), 599–610. [https://doi.org/10.1130/0016-7606\(1964\)75\(599:blsat\)2.0.co;2](https://doi.org/10.1130/0016-7606(1964)75(599:blsat)2.0.co;2)
- Yen, A., Ming, D., Vaniman, D., Gellert, R., Blake, D., Morris, R., et al. (2017). Multiple stages of aqueous alteration along fractures in mudstone and sandstone strata in Gale Crater, Mars. *Earth and Planetary Science Letters*, 471, 186–198. <https://doi.org/10.1016/j.epsl.2017.04.033>